Materials Physics and Mechanics 42 (2019) 296-310 Received: September 1, 2018

COUPLED THERMO-ELECTRO-MECHANICAL MODELING OF THERMAL FATIGUE OF SINGLE-CRYSTAL CORSET SAMPLES

A.V. Savikovskii[1*], A.S. Semenov[1], L.B. Getsov[2]

[1]SPBPU, Polytechnicheskaya 29, Russia

[2]NPO CKTI, Polytechnicheskaya 24, Russia

*e-mail: temachess@yandex.ru

Abstract. The possibilities of predicting thermal fatigue durability for single crystal on the base of coupled thermo-electro-mechanical finite-element modeling with using of deformational criterion and microstructural models of inelastic deformation are investigated. Results of thermal and stress-strain state simulations of single-crystal corset specimens under cyclic electric heating and cooling are presented and discussed. Comparison of computational results with experimental data for various single-crystal nickel-based superalloys demonstrates a good accuracy in the prediction of the number of cycles for the macrocrack initiation. The influence of maximum / minimum values of temperature in cycle and delay duration on the number of cycles for the macrocrack initiation are analyzed. The simplified analytic approximation for thermal fatigue durability curves is proposed.

Keywords: thermal fatigue, single-crystal nickel based superalloy, deformation criterion, corset sample, thermo-electric problem, finite element modeling

1. Introduction

Single-crystal nickel based superalloys [1] are used for manufacturing of blades of gas turbine engines (GTE). These materials have a pronounced anisotropy of properties and sensitivity to crystallographic orientation. The thermal fatigue strength of single crystal superalloys for various crystallographic orientations is not studied very well. For investigation of thermal fatigue durability under a wide range of temperatures with and without intermediate delays the experiments are carried out on corset (plane) specimen on the installation developed in NPO CKTI [2] (see Fig. 1). Fixed in axial direction by means of two bolts with a massive foundation a corset sample (see Fig. 2) is heated cyclic by passing electric current through it. During cycling the maximum and minimum temperatures are automatically maintained constant.

The aims of the study are: (I) to investigate numerically a process of heating and cooling of the corset sample and to obtain analytical approximation of this process, (II) to study numerically a stress-strain state of the sample during cyclic heating and cooling due to its clamping and (III) to study systematically the effect of delay at maximum temperature on the thermal fatigue durability on the base of the deformation criterion [3-5] of thermal-fatigue failure for single crystal superalloys using the results of finite element (FE) simulation of full-scale experiments. The results of simulation and their verification are obtained for the different single-crystal nickel-based superalloys: VZhM4, VIN3 and ZhS32.

http://dx.doi.org/10.18720/MPM.4232019_5

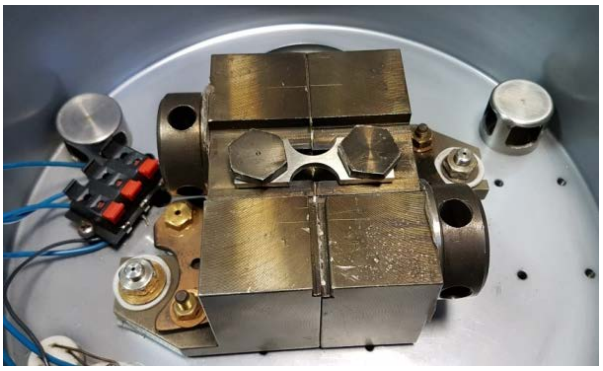

Fig. 1. Testing setup for thermal fatigue experiments

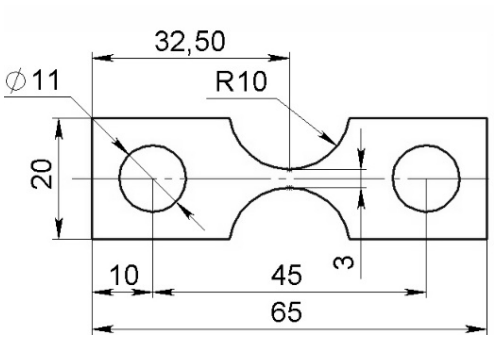

Fig. 2. Geometrical parameters of the corset sample

2. Results of numerical thermo-electric nonstationary analysis and analytical approximation for temperature changing during time

Modeling of a heating process by an electric current and a cooling process without an electric current of the corset sample has been performed with help of the FE program ANSYS with taking into account a temperature dependence of all material properties, thermos-electric contacts between the sample and an equipment, nonstationary Joule heating, convective heat exchange and radiative heat transfer between the sample and the environment. The full-scale FE model (¼ due to symmetry) of experimental object including discrete models of the specimen and equipment is presented in Fig. 3.

The simulations have been performed for single-crystal superalloys VZhM4, VIN3 and ZhS32. The properties of three alloys were accepted the same because of lack of information about nickel alloys properties dependence on temperature.

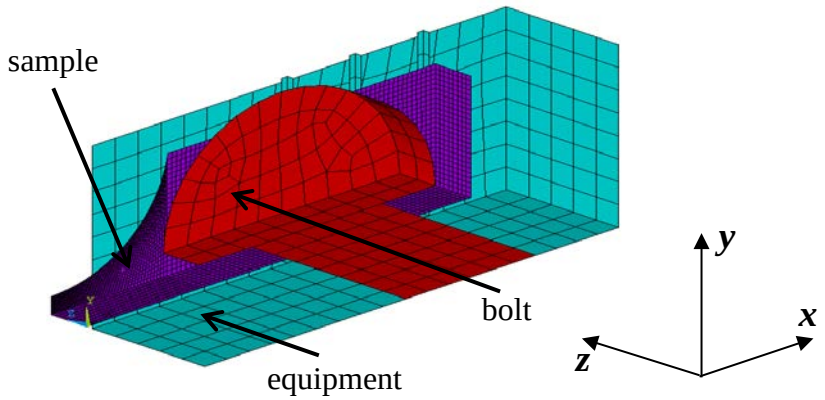

Fig. 3. Finite-element model of the corset sample with taking into account of equipment for the solution of thermo-electric problem

Modeling of heating and cooling processes of sample is carried out for five loading regimes (modes), which will be denoted further by indicating the minimum and maximum temperature of the cycle:

- 100÷800°C, a heating time is 19 s, a cooling time is 46 s;
- 150÷900°C, a heating time is 42 s, a cooling time is 59,5 s;
- 250÷1000°C, a heating time is 80 s, a cooling time is 10 s;
- 500÷1050°C, a heating time is 14 s, a cooling time is 10 s;
- 700÷1050°C, a heating time is 8 s, a cooling time is 7 s.

The material properties used in FE simulations for the single crystal nickel superalloy sample and for the steel equipment were taken from literature [6-9] (see also Tables 1-2). While specifying the properties of nickel alloy and steel the implementation of the Wiedemann-Franz's law was controlled: $\lambda \cdot \rho_e = LT$, where λ is the thermal conductivity, ρ_e is the specific electrical resistance, T is the temperature in K, L= $2.22 \cdot 10^{-8}$ W·Ω·K^{-2} is the Lorentz's constant.

Table 1. Thermo-electric properties of nickel superalloy used in simulations

T	$^{\circ}C$	**20**	**200**	**400**	**800**	**1000**	**1150**	Ref.
ρ	Kg/m^3	8550	8500	8450	8350	8330	8310	[7]
C_p	J/(kg·K)	440	520	520	570	590	600	[7]
λ	W/(m·K)	7.4	11.2	14.1	19.8	26.7	36.7	[6]
ρ_e	Ω·m	$8.7 \cdot 10^{-7}$	$9.3 \cdot 10^{-7}$	$1 \cdot 10^{-6}$	$1.2 \cdot 10^{-6}$	$1 \cdot 10^{-6}$	$8.9 \cdot 10^{-7}$	[6]

Table 2. Thermo-electric properties of pearlitic steel used in simulations

T	$^{\circ}C$	**27**	**127**	**327**	**527**	**927**	**1127**	Ref.
ρ	Kg/m^3	7778	7772	7767	7762	7754	7751	[8]
C_p	J/(kg·K)	469	506	521	660	577	530	[8]
λ	W/(m·K)	48	47	41	37	23	12	[8]
ρ_e	Ω·m	$2 \cdot 10^{-7}$	$2.6 \cdot 10^{-7}$	$4.2 \cdot 10^{-7}$	$6.4 \cdot 10^{-7}$	$1.16 \cdot 10^{-6}$	$1.4 \cdot 10^{-6}$	[9]

The coupled three-dimensional transient thermo-electrical analysis has been performed. Due to the symmetry in respect to the *xz* and *yz* planes, a quarter of the structure is considered in simulations. Thermal and electric contacts between the sample and bolts, between the sample and the foundation are taken into account. The initial temperature for the sample and the equipment is set to 30°C. For the free surface of sample the boundary condition of convective heat transfer is used:

$$q_n = h(T - T_0), \quad (1)$$

where q_n is the heat flux density, $h = 20 \frac{W}{m^2 K}$ is the coefficient of convective heat transfer, T_0 is the ambient temperature.

The condition of radiative heat transfer is also set on the surfaces of central (high temperature) part of the sample (10 mm length):

$$q_n = \varepsilon \sigma_{SB}(T^4 - T_0^4), \quad (2)$$

where ε = 0.8 is the black factor of the body, $\sigma_{SB} = 5.67 \cdot 10^{-8} W m^{-2} K^{-4}$ is the coefficient of Stefan-Boltzmann.

In order to realize an analytical approximation for the curve of temperature change in time, we consider the problem of mathematical physics of heating the sample with a constant cross-section. For example, the sample has a length and a depth the same with the corset sample 32.5 mm and 3 mm respectively, but the sample with a constant cross section has width is equal to 10 mm (Fig. 4).

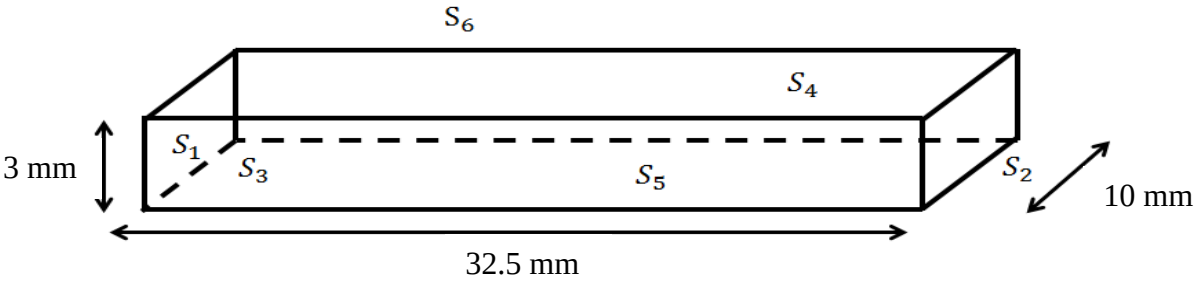

Fig. 4. The statement of simplified thermal problem

The aim of our analogy is to simplify a task of heating the corset sample to one-dimensional problem with equivalent boundary conditions. The isolation boundary conditions are set on surfaces S_3, S_4, S_5, S_6. On the surface S_2 is fixed the temperature, on the surface S_1 boundary condition of convection with a convective heat transfer coefficient h is equal to $20\frac{W}{m^2K}$. The sample in the thermal problem is heating by electric current that's why boundary condition of heat generation is set on the sample is equal to some constant Q, which does not depend on time. The equation of unsteady thermal conductivity can be represented as [10]:

$$\Delta T - \frac{\partial T}{\partial \tau} = -\frac{Q}{\lambda}, \quad (3)$$

where T is the temperature, Δ is the Laplace operator, $\tau = \frac{\lambda t}{C_\rho \rho}$ is the slow time, Q is the heat generation, λ, C_ρ, ρ are the conductive coefficient, the specific heat and the density respectively. Considering that boundary conditions in the axis y and z are a lack of heat flux and overwriting the Laplacian in Cartesian coordinates, we come to the equation:

$$\frac{d^2T}{dx^2} - \frac{\partial T}{\partial \tau} = -\frac{Q}{\lambda}, \quad (4)$$

where x is the axial coordinate along the sample. Representing T as a sum of two functions $T_1(x)$ and $T_2(x, \tau)$, we come to two equations. One of these equations has two variable, coordinate x and time τ:

$$\frac{\partial^2 T_2}{\partial x^2} - \frac{\partial T_2}{\partial \tau} = 0. \quad (5)$$

Using Fourier method [10], we put two equations with variables $X(x)$ and $\Omega(\tau)$ respectively. The equation for the variable X is:

$$X'' + \beta X = 0, \quad (6)$$

where β is the arbitrary constant. Boundary conditions for the equation (6) are a convective boundary condition in the middle of the sample and temperature is equal to zero on the edges. Also the equation with a variable Ω is:

$$\Omega' + \beta\Omega = 0. \quad (7)$$

Finding a solution of equation (6) as a sum of sinus and cosine with constants and substituting boundary conditions we put a transcendental equation:

$$\mathrm{tg}\, \gamma_n = -\frac{\lambda \gamma_n}{hl}, \quad (8)$$

where $\gamma_n = \sqrt{\beta_n} l$, $h = 20\frac{W}{m^2K}$, $l = 32.5$ mm. General solution of equation (7) is $\Omega = Ce^{-\beta_n \tau}$, where β_n is the eigenvalue and $\beta_n = \frac{\gamma_n{}^2}{l^2}$. As a result, we get $T_2(x, \tau) = C \cdot X(x) \cdot e^{-\frac{\gamma_n{}^2}{l^2}\tau}$, where γ_n can be found from an equation (8). We use simple approximation for temperature changing in time for a heating and cooling as one exponential with exponent $-\frac{\gamma_n{}^2}{l^2}$ with constants. Returning to usual time t, we can rewrite an analytical approximation for heating as:

$$T = A - B \cdot \mathrm{e}^{-\frac{\gamma_n{}^2}{l^2} \cdot \frac{\lambda}{C_\rho \rho} t}, \quad (9)$$

where *A* and *B* are constants, which are selected from conditions of equality in the beginning of the heating to minimum temperature in the cycle and in the end of the heating to maximum temperature in the cycle, γ_n can be found from a transcendental equation (8), *l* is the length of the sample. For a process of the cooling of the sample the similar analytical approximation is introduced:

$$T = C + D \cdot e^{-\frac{\gamma_n^2}{l^2}\cdot\frac{\lambda}{C_\rho \rho}t}. \quad (10)$$

Signs before constants *B* and *D* in (9) and (10) provide positive values of *B* and *D*.

Material constants λ, C_ρ, ρ are set to $20\frac{W}{mK}$, $550\frac{J}{kg\cdot K}$ and $8400\ \frac{Kg}{m^3}$ respectively. Comparison of experimental data, computational results and analytical approximation for temperature changing in time are presented in Fig. 5 for loading regimes 100÷800, 150÷900, 500÷1050 and 700÷1050 °C.

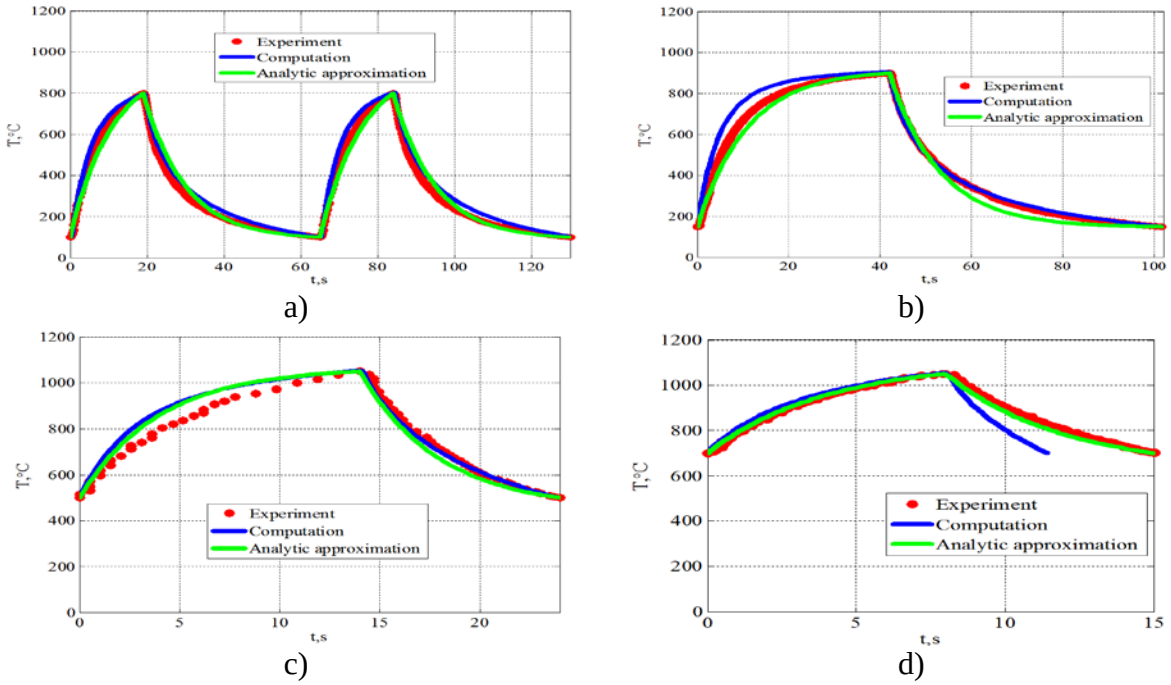

Fig. 5. Comparison of experimental data, simulation results and analytical approximation for temperature modes:
a) 100÷800°C, a heating time is 19 s, a cooling time is 46 s;
b) 150÷900°C, a heating time is 42 s, a cooling time is 60 s;
c) 500÷1050°C, a heating time is 14 s, a cooling time is 10 s;
d) 700÷1050°C, a heating time is 8 s, a cooling time is 7 s

Comparison of experimental data and computational results for temperature distribution along the corset sample at cycle phase with maximum temperature and also for the different times for loading regimes 150÷900, 250÷1000, 500÷1050 and 700÷1050°C are shown in Fig. 6.

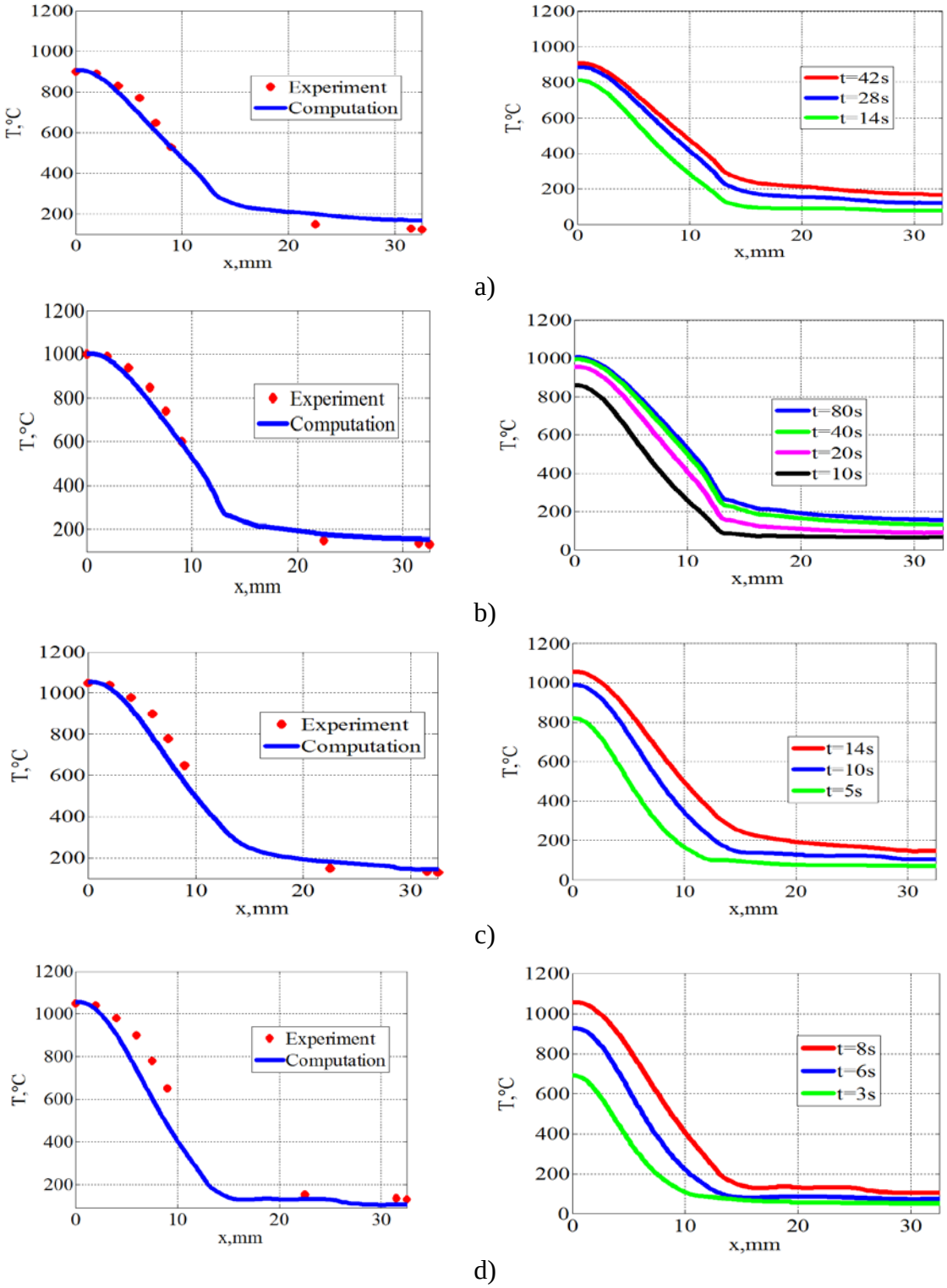

Fig. 6. Temperature distribution along the corset sample at cycle phase with maximum temperature (left) and also for the different times (right) for loading regimes: a) 150÷900°C, a heating time is 42 s, b) 250÷1000°C, a heating time is 80 s; c) 500÷1050°C, a heating time is 14 s, d) 700÷1050°C a heating time is 8 s

Temperature field distributions for cycle phase with maximum temperature for loading modes 100÷800, 150÷900, 250÷1000 and 700÷1050°C are presented in Fig. 7.

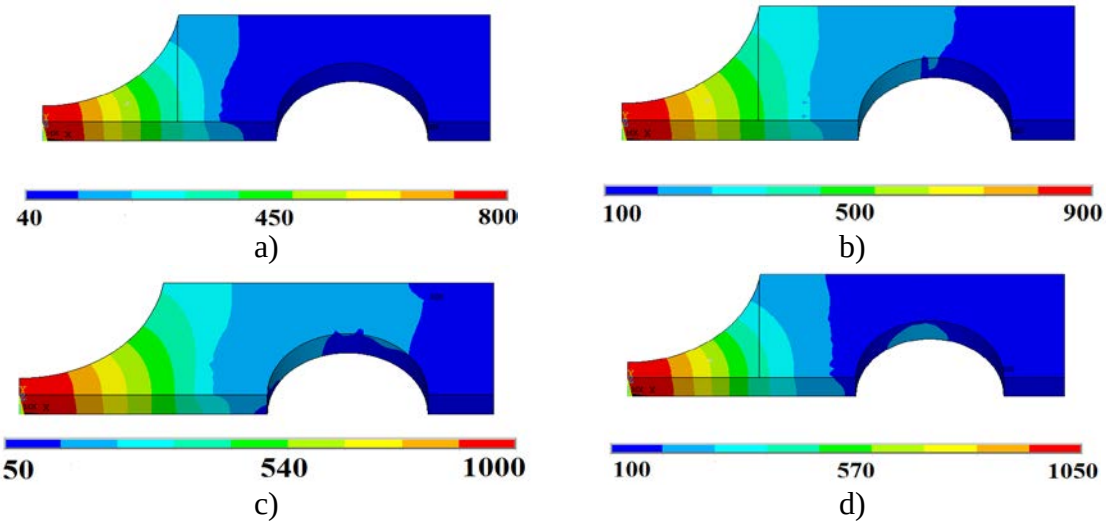

Fig. 7. Temperature field distributions for maximum temperature for loading regimes:
a) 100÷800°C; b) 150÷900°C; c) 250÷1000°C; d) 500÷1050°C

The results of thermo-electric problem simulations in form spatial and temporal distribution of the temperature field are the base for the strain and stress field computation within the framework of thermo-elasto-visco-plastic problem.

3. Results of thermo-elasto-visco-plastic analysis

The axial fixing of the corset specimen under heating leads to the high axial stress and inelastic strain appearance. The local strain and stress concentration is observed in the central part of the corset sample. The numerical simulation is required for the computation of inhomogeneous stress and inelastic strain fields in sample. Modeling and simulation of inelastic cyclic deformation of corset samples has been performed by means of the FE programs ANSYS and PANTOCRATOR [11], which allows to apply the micromechanical (microstructural, crystallographic, physical) models of plasticity and creep for single crystals [12,13]. The micromechanical plasticity model accounting 12 octahedral slip systems with lateral and nonlinear kinematic hardening [12] is used in the FE computation for the simulation single crystal superalloy behavior under cyclic loading. The Norton power-type law is used to describe creep properties.

Modeling of inelastic deformation in the corset samples has been performed with taking into account of the temperature dependence of all material properties, anisotropy of mechanical properties of single crystal sample, inhomogeneous nonstationary temperature field, mechanical contacts between bolt and the specimen, between specimen and foundation, friction between the contact surfaces, temperature expansion in the specimen and foundation. The viscous properties are taken into account because of high temperature despite a quick time of heating and cooling of the corset samples.

The two FE formulations for the thermo-mechanical problem have been considered:

- FE model with taking into account equipment;
- FE model without taking into account equipment (simplified formulation [14] for the sample only).

Using of the second formulation provides significant saving computational time due to reduction in the number of degrees of freedom and refusal to solve a contact problem. It is very actual for the numerous multivariant computations for different regimes of loading and the crystallographic orientations. One of the aims of the investigations is the selection of the equivalent (effective) length of the sample for the simplified formulation. The validity of the

simplified formulation is based on the comparison with the results of full-scale formulation (with taking into account equipment), as well as on the comparison with the relative displacements of two markers measured in experiments.

In the general case there is no symmetry in the problem (Fig. 8b) due to anisotropy of mechanical properties of single crystal sample. However in the important for practice case of [001] crystallographic orientation of sample the symmetry in respect to planes *xz* and *yz* (see Fig. 8a) can be introduced. Equipment and bolts are modeled by linear elastic material (steel), and for the sample elasto-visco–plastic model of material is used. The problem is solved in a three-dimensional quasi-static formulation. As boundary conditions the symmetry conditions are set: zero displacements on the *y*-axis on the *xz* plane and zero displacements on the *x*-axis on the *yz* plane. On the lower side of the equipment zero displacements along the *x* and *z* axes are set. On the bolt cap the pressure of 100 MPa has been applied that is equivalent to the tightening force of the bolt. The temperature boundary conditions are set from the experimental data at maximum and minimum temperature with linear interpolation in time. The mechanical properties for the alloys VZHM4 and VIN3 are taken from the papers [15,16] and for ZHS32 from [17] are presented in Tables 3-5. The mechanical properties of bolts are taken for pearlitic steel [9].

Table 3. Mechanical properties of VZHM4 used in simulations [15]

T	**˚C**	**20**	**700**	**800**	**900**	**1000**	**1050**
E_{001}	MPa	130000	101000	96000	91000	86000	82000
ν	-	0.39	0.42	0.422	0.425	0.428	0.43
α	1/K	$1.11\cdot10^{-5}$	$1.68\cdot10^{-5}$	$1.74\cdot10^{-5}$	$1.87\cdot10^{-5}$	$2.1\cdot10^{-5}$	$2.3\cdot10^{-5}$
σ_{Y001}	MPa	846	950	-	-	-	820
n	-	8	8	8	8	8	8
A	$MPa^{-n}s^{-1}$	$1\cdot10^{-42}$	$3\cdot10^{-31}$	$1\cdot10^{-29}$	$1\cdot10^{-28}$	$2\cdot10^{-27}$	$1\cdot10^{-26}$

Table 4. Mechanical properties of VIN3 used in simulations [16]

T	**˚C**	**20**	**500**	**700**	**900**	**1000**	**1050**
E_{001}	MPa	126000	110000	104000	89000	80000	75000
ν	-	0.39	0.41	0.42	0.42	0.425	0.428
α	1/K	$1.21\cdot10^{-5}$	$1.33\cdot10^{-5}$	$1.4\cdot10^{-5}$	$1.5\cdot10^{-5}$	$1.57\cdot10^{-5}$	$1.6\cdot10^{-5}$
σ_{Y001}	MPa	555	800	930	910	645	540
n	-	8	8	8	8	8	8
A	$MPa^{-n}s^{-1}$	$1\cdot10^{-42}$	$4\cdot10^{-34}$	$1.5\cdot10^{-30}$	$5.8\cdot10^{-27}$	$3.5\cdot10^{-25}$	$1.5\cdot10^{-24}$

Table 5. Mechanical properties of ZHS32 used in simulations [17]

T	**ºC**	**20**	**700**	**800**	**900**	**1000**	**1050**
E_{001}	MPa	137000	110000	105000	99800	94800	92300
ν	-	0.395	0.4248	0.4284	0.4317	0.4347	0.4361
α	1/K	$1.24\cdot10^{-5}$	$1.6\cdot10^{-5}$	$1.7\cdot10^{-5}$	$1.81\cdot10^{-5}$	$2.22\cdot10^{-5}$	$2.42\cdot10^{-5}$
σ_{Y001}	MPa	919	904	901	895	670	580
n	-	8	8	8	8	8	8
A	$MPa^{-n}s^{-1}$	$1\cdot10^{-42}$	$2.5\cdot10^{-31}$	$8.5\cdot10^{-30}$	$2\cdot10^{-28}$	$6\cdot10^{-27}$	$7\cdot10^{-26}$

In simplified formulation (see Fig. 8c) we consider only the sample without equipment, in which zero displacements on the symmetry planes *xz* and *yz* are set, the outer face of the sample parallel to the symmetry plane *xz* was fixed in the direction of the axis *x*. To exclude solid body motions, a number of points on this face are also fixed in the direction of the *y* and *z* axes.

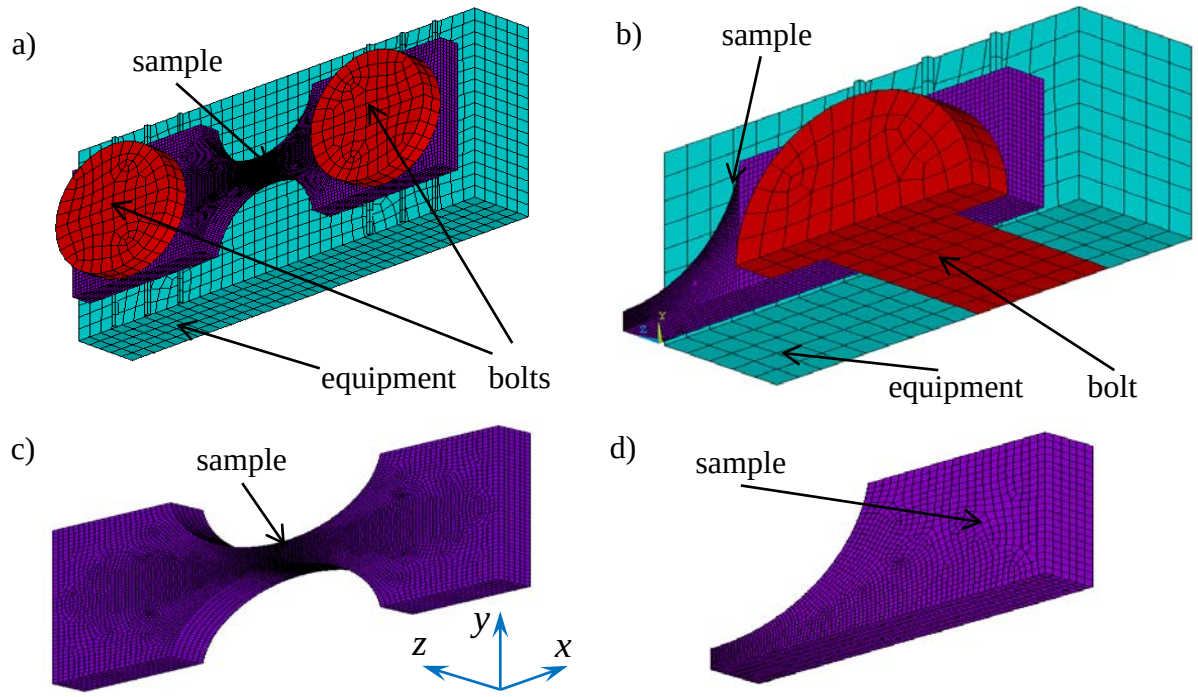

Fig. 8. FE models of the corset sample for thermo-elasto-visco-plastic problem solution:
a) full model with taking into account equipment (no symmetry),
b) model (¼ due to symmetry) with taking into account equipment,
c) simplified model without taking into account equipment (no symmetry),
d) simplified model (¼ due to symmetry) without taking into account equipment

Figure 9 shows distributions of plastic strain intensity field for three nickel superalloys and three different temperature modes after 7 cycles (for VZHM4 and VIN3 the effective length of the sample is 42 mm, for ZHS32 is 50 mm) obtained with using the FE model (¼ due to symmetry) with taking into account equipment (Fig. 8b).

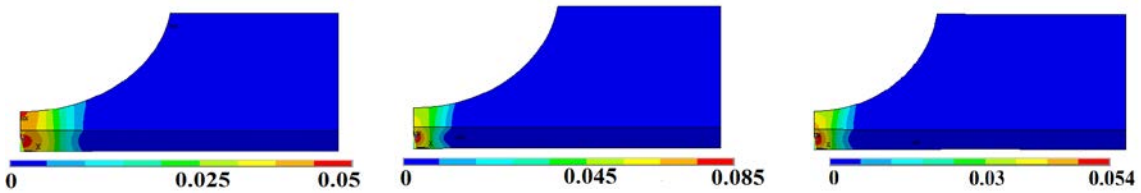

Fig. 9. Distributions of plastic strain intensity field after 7 cycles in the corset sample for:
a) superalloy VZhM4, loading regime 700÷1050°C;
b) superalloy VIN3, loading regime 500÷1050°C;
c) superalloy ZhS32, loading regime 150÷900°C

The Table 6 shows the equivalent (effective) length of the sample for the simplified formulation for different alloys, which has been found by the comparison with full model using the condition of equality of the inelastic strain ranges. FE simulations show that the

effective length doesn't depend on the type of hardening (isotropic and kinematic) and doesn't depend on temperature mode. In the FE simulations with acceptable engineering accuracy can be used the value 40 mm. Effective length takes into account the compliance of equipment and its variation in considered range has no appreciable on the results.

Table 6. The equivalent length of the corset sample for different alloys

VZHM4	VIN3	ZHS32
34-42 mm	38-46 mm	40-52 mm

4. Influence of the delay on the thermal fatigue durability

FE computations are carried out for a part of a corset sample (simplified FE model with effective length of sample equal 40 mm, see Fig. 8d). The temperature fields are set from the experimental data at maximum and minimum temperature cycle phase with using linear interpolation in time.

The influence of the delay at maximum temperature on the number of cycles to the formation of macrocrack is analyzed in the range from 1 min to 1 hour for the cyclic loading regimes with:

- maximum temperature of 1100°C and a temperature range of 900°C;
- maximum temperature of 1050°C and a temperature range of 550°C;
- maximum temperature of 1050°C and a temperature range of 350°C;
- maximum temperature of 1000°C and a temperature range of 750°C;
- maximum temperature of 900°C and a temperature range of 750°C.

The heating times in the cycle are 24s, 7s, 18 s, 28s, the cooling time are 15s, 15s, 40s, 52s for VZhM4. The heating time in the cycle is 10 s, the cooling time is 16s for VIN3. The heating times in the cycle is 25 s, the cooling time is 75s for ZhS32.

The mechanical properties for the alloys VZhM4 and VIN3 were taken from the papers [15], [16] and for ZhS32 from [17] (see also Tables 3-5).

The problem is solved in a quasi-static 3-dimensional formulation. The FE model is shown in Fig. 8d. The boundary conditions are zero displacements in the direction of the *x*-axis on two side faces of the sample with the normal along the *x*-axis. To exclude rigid body motions, a number of points on these faces in the direction of the *y* and *z* axes are also fixed.

Temperature evolutions in central point of sample with and without delay for loading regimes 700÷1050°C, 500÷1050°C, 250÷1000°C and 150÷900°C are presented schematically in Fig. 10.

Damage calculation and estimation of the number of cycles for the macrocrack initiation are made on the basis of four-member deformation criterion [3-5]:

$$D = \sum_{i=1}^{N} \frac{\left(\Delta\varepsilon_{eq_i}^{p}\right)^{k}}{C_1(T)} + \sum_{i=1}^{N} \frac{\left(\Delta\varepsilon_{eq_i}^{c}\right)^{m}}{C_2(T)} + \max_{0\le t\le t_{\max}} \frac{\varepsilon_{eq}^{p}}{\varepsilon_r^{p}(T)} + \max_{0\le t\le t_{\max}} \frac{\varepsilon_{eq}^{c}}{\varepsilon_r^{c}(T)}, \tag{11}$$

where the first term takes into account the range of plastic strain within the cycle, the second term deals with the range of creep strain within the cycle, the third term is unilaterally accumulated plastic strain (ratcheting), the fourth term is unilaterally accumulated creep strain. The number of cycles to initiate macrocrack N is determined from the condition $D = 1$.

The equivalent strain for single crystal is defined by maximum shear strain in the slip system with normal to the slip plane $\mathbf{n}_{\{111\}}$ and the slip direction $\mathbf{l}_{\langle 011\rangle}$:

$$\varepsilon_{eq} = \mathbf{n}_{\{111\}} \cdot \boldsymbol{\varepsilon} \cdot \mathbf{l}_{\langle 011\rangle}. \tag{12}$$

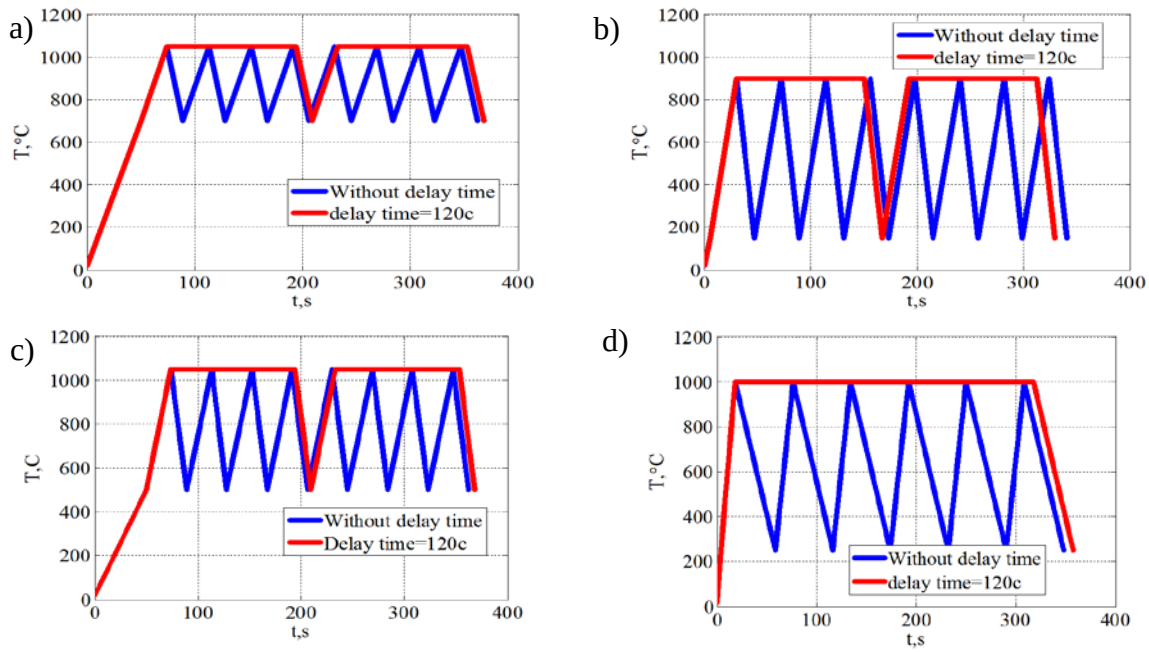

Fig. 10. Schematic presentations of temperature evolutions in central point of sample for loading regimes with and without delay:
a) 700÷1050°C; b) 150÷900°C; c) 500÷1050°C and d) 250÷1000°C

Usually it takes in (11) the values of constants: $k = 2$, $m = \frac{5}{4}$, $C_1 = \left(\varepsilon_r^p\right)^k$, $C_2 = \left(\frac{3}{4}\varepsilon_r^c\right)^m$, where ε_r^p and ε_r^c are ultimate strains of plasticity and creep under uniaxial tension. In the FE computations the values of ultimate strains $\varepsilon_r^p = \varepsilon_r^c = 17\ \%$ are used the same for all considered alloys. Improvement of the prediction accuracy of the delay time influence on durability can be achieved by the refinement of the constant strains ε_r^p on the basis of data without delay.

An analytical approximation of delay time influence in thermal fatigue strength has been proposed in the form:

$$N = N_{\min} + (N_0 - N_{\min}) \cdot e^{-t_{delay}/\tau}, \qquad (13)$$

where N is the number of cycles to crack initiation as function of delay time t_{delay}, N_0 is the computational number of cycles in case without delay time, $N_{\min}$ is the number of cycle in case with delay time is equal to 1 hour, τ is a constant (50 s for all considered materials). Comparison of results of FE simulations with experimental data for single-crystal superalloys VZhM4, VIN3 and ZhS32 is given in Fig. 11. The good agreement between computational and experimental results is observed.

Comparison of results of FE simulations and analytical approximation (13) concerning the effect of the delay time at the maximum temperature on the thermal fatigue durability for single-crystal superalloys VZhM4, VIN3 and ZhS32 is given in Fig. 12. Small deviations are observed only in the vicinity of the region of maximum curvature.

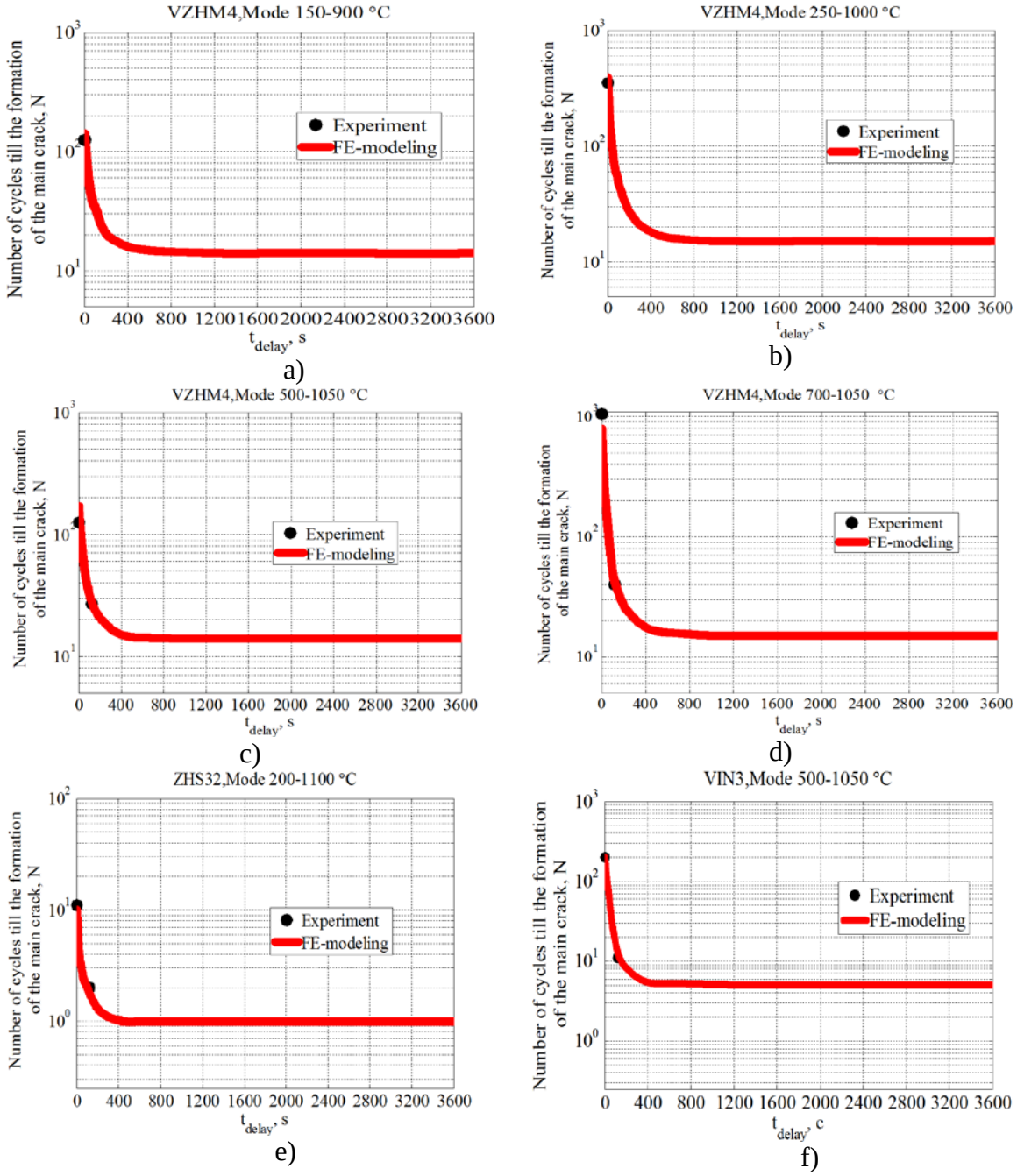

Fig. 11. Comparison of results of FE simulations and experimental data for alloys:
a) VZhM4, loading regime 150÷900°C, a heating time is 28 s, a cooling time is 52 s;
b) VZhM4, loading regime 250÷1000°C, a heating time is 18 s, a cooling time is 40 s;
c) VZhM4, loading regime 500÷1050°C, a heating time is 24 s, a cooling time is 15 s;
d) VZhM4, loading regime 700÷1050°C, a heating time is 7 s, a cooling time is 15 s;
e) ZhS32, loading regime 200÷1100°C, a heating time is 25 s, a cooling time is 75 s;
f) VIN3, loading regime 500÷1050°C, a heating time is 10 s, a cooling time is 16 s

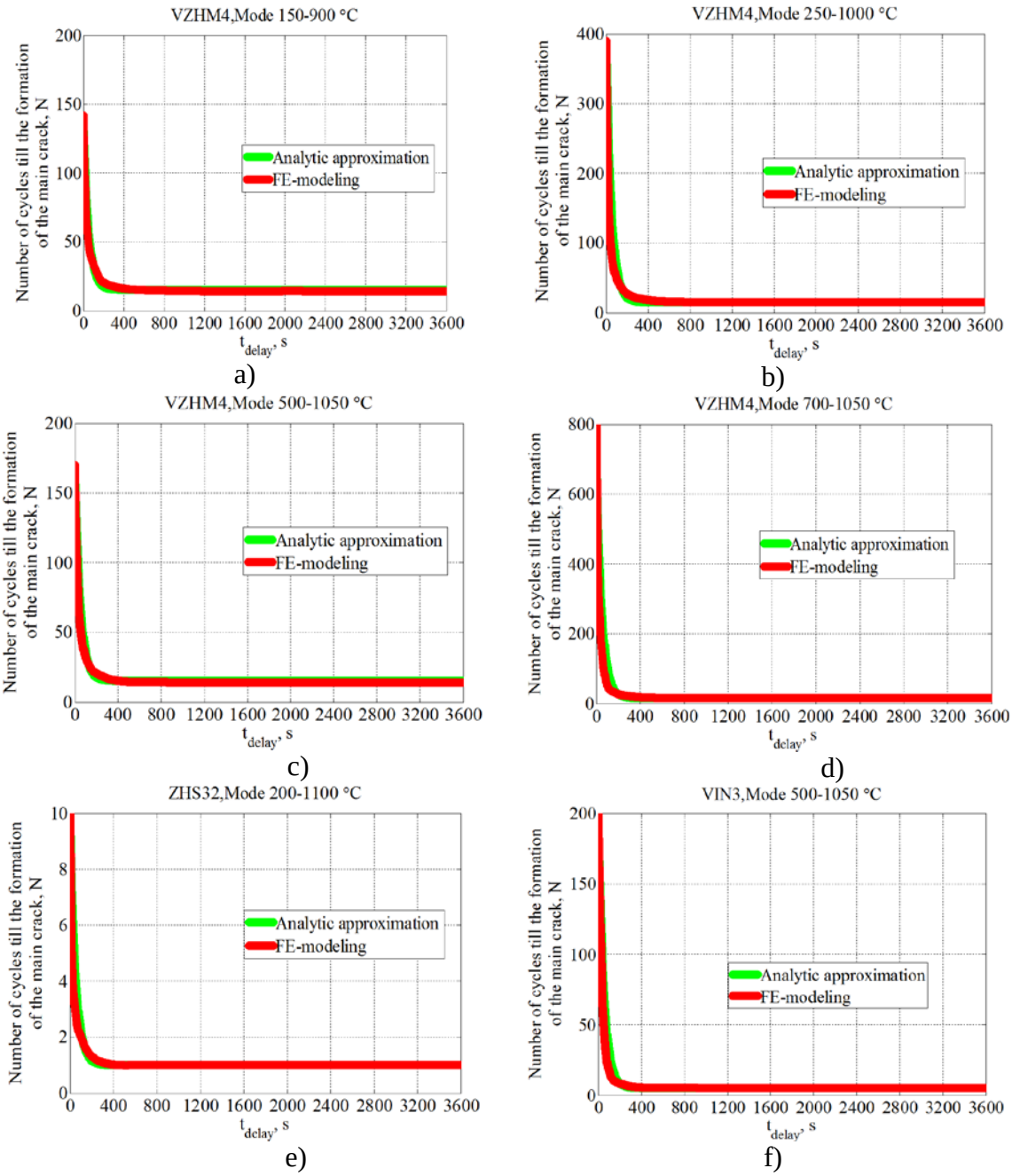

Fig. 12. Comparison of results of FE simulations and analytical approximation (13) for alloys:
a) VZhM4, loading regime 150÷900°C, a heating time is 28 s, a cooling time is 52 s;
b) VZhM4, loading regime 250÷1000°C, a heating time is 18 s, a cooling time is 40 s;
c) VZhM4, loading regime 500÷1050°C, a heating time is 24 s, a cooling time is 15 s;
d) VZhM4,loading regime 700÷1050°C, a heating time is 7 s, cooling time is 15 s;
e) ZhS32, loading regime 200÷1100°C, a heating time is 25 s, a cooling time is 75 s;
f) VIN3, loading regime 500÷1050°C, a heating time is 10 s, a cooling time is 16 s

5. Conclusions

The results of thermal and stress-strain state simulations for single-crystal corset specimens under cyclic electric heating show a good agreement with the experimental data for a wide range of temperature alteration and different single-crystal nickel based superalloys. Obtained results point out on the possibility of predicting thermal fatigue durability for single crystal by

means of thermo-electro-mechanical finite-element simulation with using of four-member deformational criterion of damage accumulation and microstructural models of inelastic deformation.

A systematic numerical analysis of the delay effect at maximum temperature on thermal fatigue durability was carried out for various single-crystal superalloy samples in wide range temperatures. The simplified analytic approximation for durability curves are proposed on the base of results of multivariate computational experiments.

Acknowledgments. *Research was conducted under the financial support of the Russian Science Foundation, Grant no. 18-19-00413.*

References

[1] Shalin RE, Svetlov IL, Kachanov EB, Toloraiya VN, Gavrilin OS. *Single crystals of nickel heat-resistant alloys.* Moscow: Mashinostroenie; 1997. (In Russian)

[2] Getsov LB. *Materials and strength of gas turbine parts.* Rybinsk: Gazoturbinnye Tekhnologii; 2010. (In Russian)

[3] Getsov LB, Semenov AS. Criteria of fracture of polycrystalline and single crystal materials under thermal cyclic loading. In: *Proceedings of CKTI. Vol. 296.* 2009. p.83-91.

[4] Semenov AS, Getsov LB. Thermal fatigue fracture criteria of single crystal heat-resistant alloys and methods for identification of their parameters. *Strength of Materials*. 2014;46(1): 38-48.

[5] Getsov LB, Semenov AS, Staroselsky A. A failure criterion for single-crystal superalloys during thermocyclic loading. *Materials and technology*. 2008;42(1): 3-12.

[6] Petrushin NO, Logunov AV, Kovalev AI, Zverev AF, Toropov VM, Fedotov NH. Thermophysical properties of Ni_3Al-Ni_3Nb directly crystallized eutectic composition. *High temperature thermophysics*. 1976;14(3): 649-652.

[7] Zinoviev VE. *Thermo-physical properties of metals at high temperatures.* Moscow: Metallurgia; 1989. (In Russian)

[8] Chirkin VS. *Thermophysical properties of nuclear materials.* Moscow: Atomizdat; 1968. (In Russian)

[9] Maslenkov SB, Maslenkova EA. *Steels and alloys for high temperatures.* Moscow: Metallurgia; 1991. (In Russian)

[10] Courant R, Hilbert D. *Methods of mathematical physics. Vol. 2*. Leningrad: GTTI; 1945.

[11] Semenov AS. PANTOCRATOR – finite-element program specialized on the solution of non-linear problems of solid body mechanics. In: *Proc. of the V-th International. Conf. "Scientific and engineering problems of reliability and service life of structures and methods of their decision"*. Saint Petersburg: Izd-vo SPbGPU; 2003. p.466-480.

[12] Cailletaud GA. Micromechanical approach to inelastic behaviour of metals. *Int. J. Plast.* 1991;8(1): 55-73.

[13] Semenov AS. Identification of anisotropy parameters of phenomenological plasticity criterion for single crystals on the basis of micromechanical model. *Scientific and technical sheets SPbGPU. Physical and mathematical Sciences*. 2014;2(194): 15-29. (In Russian)

[14] May S, Semenov AS. Modeling of inelastic cyclic deformation of monocrystalline specimens. In: *Proc. of the XXXIX week of science of SPbPU. Vol. 5*. 2010. p.73-74. (In Russian)

[15] Kablov EN, Petrushin NO, Svetlov IL, Demonis IM. Nickel casting heat-resistant alloys of the new generation. In: *The jubilee nauch.-tech. sat. Aviation materials and technologies.* Moscow: Proceedings of VIAM; 2012. p.36-52. (In Russian)

[16] Semenov SG, Getsov LB, Semenov AS, Petrushin NV, Ospennikova OG, Zhivushkin AA. The issue of enhancing resource capabilities of nozzle blades of gas turbine

engines through the use of new single crystal alloy. *Journal of Machinery Manufacture and Reliability*. 2016;4: 30-38.
[17] Getsov LB, Semenov AS, Tikhomirova EA, Rybnikov AI. Thermocyclic and static failure criteria for single crystal superalloys of gas turbine blades. *Materials and technology*. 2014;48(2): 255-260.